Towards LES models of jets and plumes

By A. T. Webb† AND N. N. Mansour‡

1. Motivation and objectives

As pointed out by Rodi (1982) standard integral solutions for jets and plumes developed for discharge into infinite, quiescent ambient are difficult to extend to complex situations - particularly in the presence of boundaries such as the sea floor or ocean surface. In such cases the assumption of similarity breaks down and it is impossible to find a suitable entrainment coefficient. The models are also incapable of describing any but the most slowly varying unsteady motions.

There is therefore a need for full time-dependent modeling of the flow field for which there are three main approaches - Reynolds averaged numerical simulation (RANS), large eddy simulation (LES) and direct numerical simulation (DNS). Rodi (1982) applied RANS modeling to both jets and plumes with considerable success, the test being a match with experimental data for time-averaged velocity and temperature profiles as well as turbulent kinetic energy and rms axial turbulent velocity fluctuations. This model still relies on empirical constants, some eleven in the case of the buoyant jet, and so would not be applicable to a partly laminar plume, may have limited use in the presence of boundaries, and would also be unsuitable if one is after details of the unsteady component of the flow (the turbulent eddies). At the other end of the scale DNS modeling includes all motions down to the viscous scales. Boersma *et al.* (1998) have built such a model for the non-buoyant case which also compares well with measured data for mean and turbulent velocity components. The model demonstrates its versatility by application to a laminar flow case. As its name implies, DNS directly models the Navier-Stokes equations without recourse to subgrid modeling so for flows with a broad spectrum of motions (high Re) the cost can be prohibitive - the number of required grid points scaling with $Re^{9/4}$ and the number of time steps with $Re^{3/4}$ (Piomelli and Chasnov, 1996).

The middle road is provided by LES whereby the Navier-Stokes equations are formally filtered with the filter chosen to only exclude the smallest turbulent motions. If successful, LES should provide much of the detail available to DNS but at more bearable cost. Fatica *et al.* (1994) in comparing LES with DNS for a low Reynolds number jet showed that the LES could simulate the temporally evolving behavior including growth of the jet thickness.

It is the intention of this report to explore the application of an LES model to jets and plumes. As always, before tackling complex situations, the model must be tested for the simplest of cases and so we address only two, a non-buoyant axisymmetric jet issuing steadily from an orifice into a semi-infinite stationary environment and a buoyant jet in the same environment. The work is a continuation of Basu and Mansour (1999).

† University of New South Wales, Australian Defence Force Academy
‡ NASA Ames Research Center, Moffett Field, CA

2. Numerical method

2.1. *Governing equations*

In the present study, we aim to compute the evolution of a circular jet and plume in uniform surroundings. Since the density differences away from the source of a plume are typically small compared to ambient density, we take advantage of the Boussinesq approximation, whereby the effects of density variations are neglected, except in that they are modeled by a source or buoyancy term in the momentum equations. The equations to be solved are the modified incompressible Navier-Stokes equations under the Boussinesq approximation together with the continuity equation and a scalar transport equation where for the buoyant case the scalar represents buoyancy or temperature deficit.

The non-dimensional governing parameters for this flow are:

$$\begin{aligned} \text{Reynolds number} &= Re = U_o D_o/\nu \,, \\ \text{Prandtl number} &= Pr = \nu/\kappa \,, \\ \text{Grashof number} &= Gr = g\prime_0 / D_o^3/\nu^2, \end{aligned}$$

where U_o is the mean vertical velocity of the fluid leaving the source (used to non-dimensionalize all velocities), D_o is the diameter of the orifice (used to non-dimensionalize lengths), ν is the kinematic viscosity of the fluid, κ the scalar diffusivity, and $g\prime_0$ the initial buoyancy. For the non-buoyant case, Gr is set to zero.

In the following we use T to represent the dimensionless scalar concentration (eg. pollutant, buoyancy, temperature deficit etc).

2.2. *Large eddy simulation*

To create a computational model, the LES approach is to spatially filter the Navier-Stokes/continuity/tracer equations with the filter cutoff chosen to retain the energy-containing wavenumbers. In the present study, the SGS stresses and fluxes are modeled using the dynamic approach (Germano *et al.*, 1991, Lilly, 1992, and Cabot and Moin, 1996), which automatically determines, using different filter widths, the spatial distribution of the magnitude of eddy viscosity as required by the subgrid-scale Smagorinsky model; this procedure obviates the need for any empirical determination of the Smagorinsky constant. A major attraction of this method is that it is much more likely to be successful for inhomogeneous flows, particularly in cases where part of the domain is laminar as we have in jets and plumes. This issue was explored by Liu *et al.* (1994) who compared the Smagorinsky and the dynamic models with particle image velocimetry laboratory measurements in the far field of a turbulent round jet. The Smagorinsky model was found to correlate poorly with the real turbulent stress, while the dynamic model yielded appropriate coefficients. The inadequacy of the Smagorinsky model was also demonstrated by Bastiaans *et al.* (1994) in an LES model of transient buoyant plumes in an enclosure where they found they could only get a match of the evolving plume by tuning the Smagorinsky constant. Such tuning reduces the generality of a model.

2.3. *Numerical scheme*

The numerical scheme for the Navier-Stokes/continuity equations is a fractional step method similar to that of Kim & Moin (1985) who extended the method of Chorin (1968). At the start of each step the subgrid model results are converted to a viscosity to be added to the molecular value and the corresponding diffusivity is estimated from the viscosity with a constant Prandtl number.

We use the LES code of Boersma, an adaptation of DNS code used in a study of pure jets (Boersma *et al.*, 1998). A spherical polar coordinate system $(R, \theta, \phi$; along the

radial vector, lateral and azimuthal directions respectively) is used here because, for the present flow with its conical mean growth, a spherical coordinate system allows for a well-balanced resolution of the flow field without excessive grid points. For presentation purposes, however, and for comparison to laboratory data, the results are converted to the axisymmetric cylindrical coordinate system (z axial and r radial). The symbols U and V are used for velocities in the z and r directions respectively. Further details of the computational scheme can be found in the above references.

2.4. *Boundary conditions and test parameters*

For the chosen staggered grid only velocities normal to the boundary need be specified - i.e. six components. The equation for the tracer (T) is second order in each spatial direction and so we need six boundary conditions for temperature as well.

For the bottom boundary outside the orifice, the velocity is set to zero (i.e. a solid wall). Inside the orifice the vertical velocity profile is specified as a log profile matching smoothwall pipe flow (although the wall boundary layer is not resolved). Other profiles were also tested (tophat and parabolic) with little difference in the substantive results. In addition to the prescribed inlet velocity profile we impose a random white noise perturbation of peak magnitude 2% on the axial velocity component at the inlet; this roughly corresponds to the reported fluctuation level near the inlet in the experiments of Shabbir & George (1994). Similar conditions are applied to temperature, viz tophat profile of zero outside and unity inside.

At the lateral boundary of the computational domain we apply a stress-free condition (Boersma *et al.*, 1998, Gresho, 1991) which in spherical coordinates reads:

$$-P + 2\nu\left(\frac{1}{r}\frac{\partial u_\theta}{\partial \theta} + \frac{u_R}{R}\right) = 0.$$

As adopted by Boersma *et al.* (1998) the value of P at this boundary is set to a constant value (assumed zero) representing its value at infinity. We will revisit this choice at the end of the Report.

At the outflow boundary or the top end of the current computational domain, we use the so-called advective boundary condition, which has been applied successfully by many for similar flows (e.g. Boersma *et al.*, 1998). Negative values of u_R at the outflow boundary are set to zero in order to ensure that no flow enters the computational domain from the outflow region at the top. Corresponding values of T are likewise set to zero at these points.

Periodic boundary conditions are used along the azimuthal ϕ direction boundaries and lateral velocity (u_θ) is set to mean value at $\theta = 0$.

The test conditions were originally chosen to match the particular conditions of round turbulent buoyant plume reported in Shabbir & George (1994) although we subsequently compare with a broader range of experiments. Together with the boundary conditions the following parameters completely determine the flow:

$$Re = 3500, \quad Pr = 0.7, \quad Gr = 9.25 \times 10^6 \text{ for plume, } Gr = 0 \text{ for jet.}$$

There are two points to made about these values - viz whether we would expect the flow to be turbulent and secondly for the buoyant case, at what point we would expect the buoyancy effects to dominate the initial momentum effects.

On the first issue, although there are no critical values of these parameters to guarantee turbulent flow, the value of Re is within the range of experimental data for which the plume is turbulent at or near the nozzle (see Chen and Rodi, 1980, for a discussion

on this issue). Note that for the buoyant case, the value of Gr, would not in itself be high enough to guarantee a turbulent plume. However the concomitant high Re and our random perturbation at the source do yield turbulent flow from the nozzle.

From the experiments of Ricou & Spalding (1961) transition from jet-like to plume-like behavior occurs at a dimensionless height scaled by the so-called Morton length. In our terms the scaling length is $.557/.254\sqrt{2}/\pi^{.25} D_0 Re/\sqrt{Gr} \approx 2D_0 Re/\sqrt{Gr}$, and so in our buoyant case the transition to plume occurs within about 2.5 diameters of the source.

A third issue that cannot be related quantitatively to the test parameters is the distance over which a core region characterized by the flow profile at the source persists. From experimental data this distance is of order $6D_0$ (Chen and Rodi, 1980) although fully developed jet flow may take some additional distance.

The computations are carried out in a domain that extends to 50 diameters downstream of the source. The domain encompasses a conical volume of lateral angle $\pi/12$, with a virtual origin that is 15 diameters upstream of the orifice. For the purpose of LES, this volume is discretized using a grid of size $(N_r = 128, N_\theta = 40, N_\phi = 32)$, where N_r, N_θ, N_ϕ are the number of finite-volume cells along the (r, θ, ϕ) directions respectively. The grid spacing along r increases linearly from 0.1 near the source to 0.7 near the outflow boundary. Grid spacing is maintained constant along θ and ϕ. Time stepping was chosen to satisfy CFL conditions Boersma *et al.* (1998) and for the jet model a typical time step in dimensionless time units (D_0/U_0) was 0.01 while for the plume it was 0.003. Spatially the grid is an order of magnitude smaller than the expected large scale (typically 0.4z, although there is an arbitrariness about the definition of the plume edge) and an order of magnitude larger than the Kolmogorov length scale (see Papantoniou and List, 1989) as appropriate for LES modeling. Temporally the sampling is much smaller than the Kolmogorov time scale - i.e. instantaneous.

The computations are carried out for over 100,000 time-steps (a non-dimensional time of about $t = 300$). Averaging for statistical quantities was done towards the end of the simulations when we were convinced the flow was statistically stationary. The throughput on a 195 MHz 8-processor SGI Origin 2000 is about 0.7 seconds per time step.

3. Results

3.1. *Jet imaging*

A meridional section of tracer concentration simulates a Schlieren photograph that might be captured in the laboratory and enables visualization of several features. Figure 1 is a sequence of three such sections at time steps of 7.4 dimensionless time units.

From any one of these one can see, for example, the zone of flow establishment (zfe) between $z = 0$ and $z \approx 7$. The dark central region with concentration of unity represents source fluid, the edge of which is being eroded by vortices whose dimensions are quite large compared to the nozzle diameter. These vortices grow until they encompass the full radius of the source fluid core. Moreover, there is a regularity in these vortices that results in pulses of higher than locally averaged concentration that advect away from the zfe.

The arrow in the three images follows an eddy apparently in the process of engulfing a patch of ambient fluid. This large scale process is distinctly different from an image implied by integral models of a smooth diffusion process whereby there would be a gradual increase in concentration from the jet edge to the center. Engulfing eddies can be seen

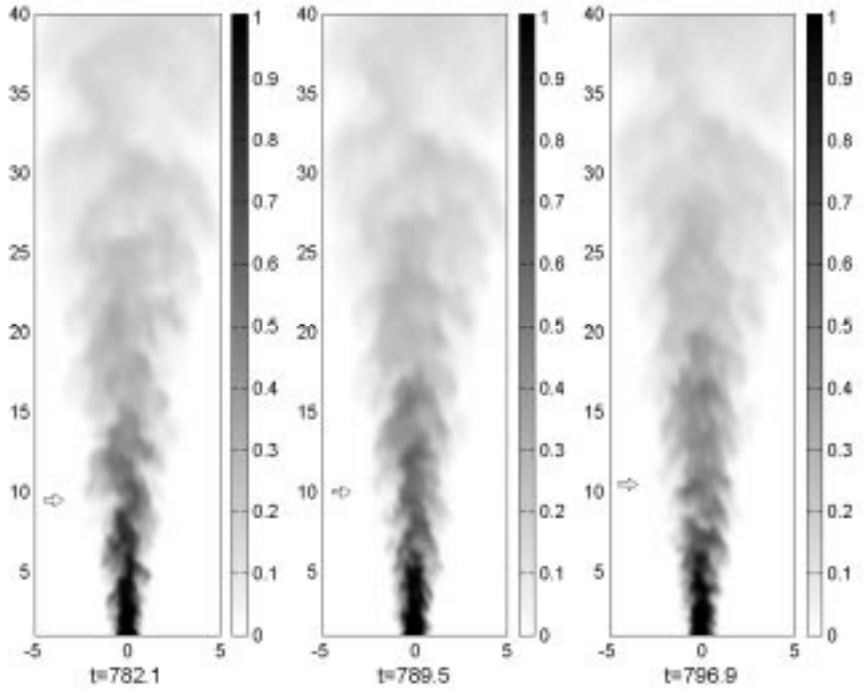

FIGURE 1. A sequence of meridional tracer slices. The arrows track a particular eddy as it engulfs ambient fluid.

throughout the images with speed decreasing and size increasing with distance (z) from the origin.

3.2. *Quantifying scale*

The apparent underlying regularity in the image sequence suggests that we can seek a reliable way of defining time and space scales for the dominant eddies. For time, the obvious method is to look for a spectral peak computed from a time series and indeed when that is done one finds a clear peak somewhat higher than the expected large scale frequency but much lower than the Kolmogorov frequency.

One could invoke the Taylor frozen-field assumption to deduce a spatial scale but an impediment to computing such a scale is the obvious inhomogeneity. However we can make use of the scaling determined from the mean and variance to transform an axial sample of the tracer to a homogeneous equivalent. Subtracting the mean centerline temperature and then dividing by the mean removes these two trends but still leaves a z-dependent wavelength. However if we transform the z-axis by the antiderivative of the expected inverse growth rate the z-dependence is removed. In this case the growth is expected to be linear and hence the transformation is simply logarithmic. A sample centerline record and its transformed homogeneous equivalent are shown in Fig. 2. The spectra of 100 such records were averaged to yield the spectrum shown in Fig. 3. The interpretation of the peak at 5 transformed wave number units is that the centerline eddy length is equal to $0.2z$. This provides a definitive measure of the large scale motions and may be a better representation than the plume width with its uncertainty in definition.

The small peaks to the right of the peak are not due to uncertainty in the spectral estimates. Rather they arise because of the asymmetry of the shape of the puffs. This

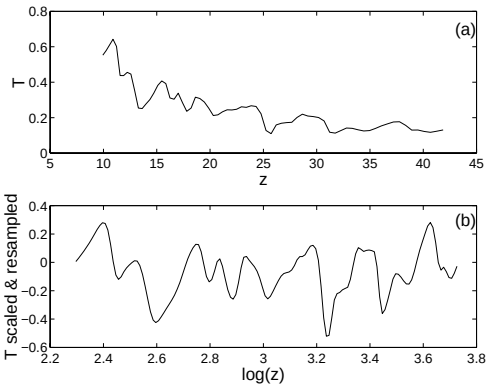

FIGURE 2. A sample centerline temperature trace (a) and its equivalent (b) after transforming to homogeneous form

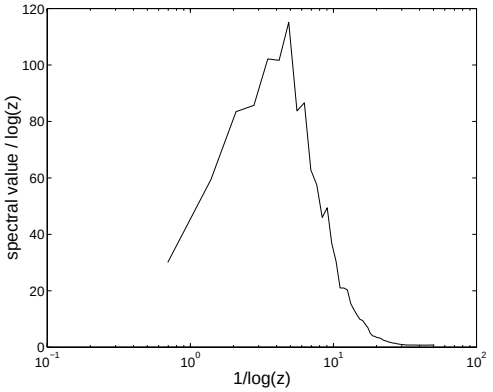

FIGURE 3. Spectrum of centerline scalar in homogeneous transformed space

feature can be clearly seen in the transformed centerline trace (Fig. 3b) where the front of an advancing eddy is typically steeper than the back. The manifestation of this feature in the spurious spectral peaks was confirmed by finding the spectrum of an artificial asymmetrical wave shape (results not shown here).

3.3. *Comparisons with laboratory data*

To have confidence in the exploration of scale we must be assured that the model is producing reliable results and one way of doing that is by comparing with laboratory data. There is a wealth of such data and we use a selection reviewed by List (1982). The data represent air in air and water in water. Despite the range of fluids and laboratory conditions there is a surprising consistency between the results and hence we would expect our model to be able to match them well.

To produce the model results for comparison we have averaged first moment and second moment statistics (third moment statistics were also computed but are not shown here) over many snapshots. For the results shown here a total of 324 snapshots spaced at 100 timesteps were used. The data were also averaged azimuthally so we have a total of about 10000 samples and if they were independent, the uncertainty for a mean quantity (such as the centerline axial velocity) would be about 0.3%. Now the samples are far from uncorrelated (particularly the azimuthal values) but even discounting the azimuthal averaging gives an uncertainty estimate of 2%.

3.3.1. *Mean flow statistics*

Here we examine two statistics, the mean z-direction velocity (U) and the tracer concentration (T). The procedure for reducing the data was to fit Gaussian curves (using Matlab's routine nlinfit with emphasis on the inner radius) to the r-direction profiles. The fitted e-folding radius (r_e) and the fitted maximum value were used to scale the data. A typical collapse of the data is given in Fig. 4 along with the fitted Gaussian. There are two checks we can perform on this data - that the centerline value of U or T decays as z^{-1} and that the jet e-folding width grows linearly at $0.107z$ for U and $0.126z$ for T. The uncertainty for the growth rates is 3% for both U and T (List, 1982).

The model centerline averages (Fig. 5) show an initial region of approximate length 4 where there is little change from the source value. The decay profile then steepens until

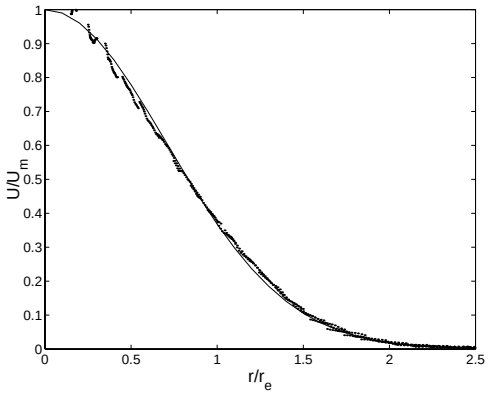

FIGURE 4. Collapse of average axial velocity. The points represent scaled axial velocities at a range of z-positions. The solid line is the common fitted Gaussian profile.

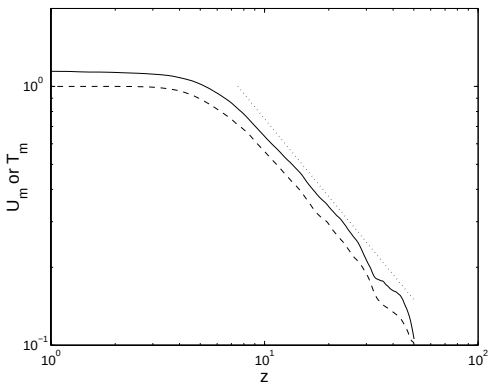

FIGURE 5. Centerline mean velocity (solid) and scalar(dashed). The dotted line is a slope of z^{-1} as found from laboratory data for both U_m and T_m

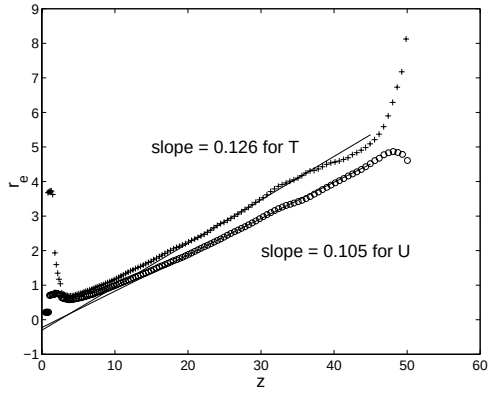

FIGURE 6. Growth of plume width in terms of the e-folding width for z-direction velocity (circles) and tracer (crosses).

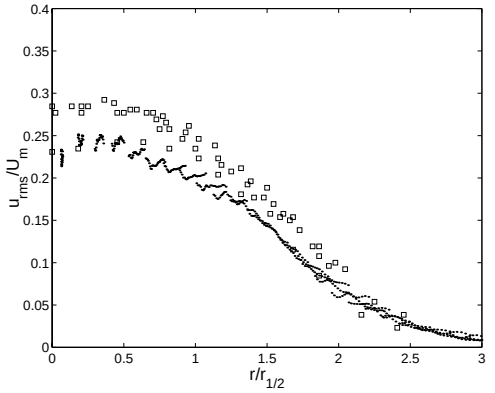

FIGURE 7. z-direction velocity rms fluctuations scaled by centerline mean velocity. The model results are the points, while laboratory results from a variety of sources reviewed by List (1982) are represented by the open boxes.

it approaches something like a constant slope. The effect of an imperfect downstream boundary condition is evident in the region beyond about 30. For both U and T the slope approaches z^{-1} as expected from the laboratory results.

We choose the segment between $z = 20$ and $z = 30$ where the centerline most closely matches the expected value to check for the width growth rate (Fig. 6). The matches are remarkably close to the laboratory data and well within the data uncertainty. The poor Gaussian fit in the zfe and the influence of the downstream boundary are also evident in these plots.

3.3.2. *Turbulent statistics*

If we were only interested in mean flow information, there would be no point in using anything but the asymptotic models. But we are also interested in the variability as given by the second moment statistics. Of the many such statistics that were computed we

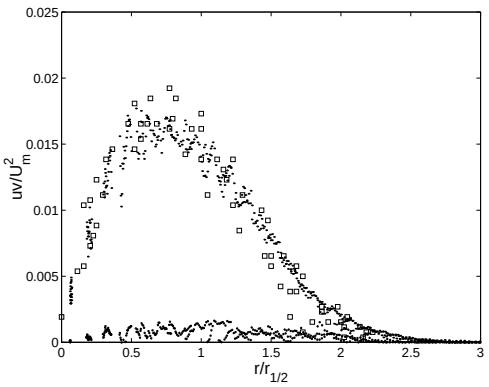

FIGURE 8. Turbulent flux scaled by square of centerline mean velocity. The symbols match Fig. 7. The additional points (small open circles) near the bottom are the subgrid contribution.

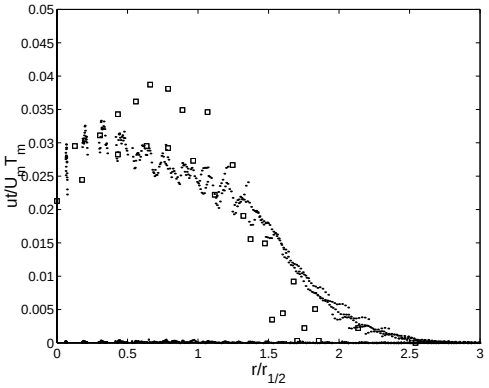

FIGURE 9. Turbulent scalar transport scaled by centerline mean velocity and scalar concentration. The symbols match Fig. 8.

present only three – the z-velocity fluctuations, $u_{rms} = \sqrt{\overline{u\prime^2}}$, the turbulent momentum transport, $uv = \overline{u\prime v\prime}$ (v is the r-direction velocity) and the turbulent scalar transport $uT = \overline{u\prime T\prime}$.

For an LES model we would expect the resolved field to provide most of the variance information and we can check that by computing subgrid scale estimates at least for the two transport statistics using $uv_{sg} = \overline{\nu_{sg}(\frac{\partial U}{\partial r} + \frac{\partial V}{\partial z})}$ and $uT_{sg} = \overline{\nu_{sg}(\frac{\partial T}{\partial z})/Pr}$.

As for the mean statistics we scale these data using centerline velocities and scalars as appropriate. The radius is also scaled, although to match the data quoted by List (1982) we use $r_{1/2}$, the point at which the velocity is half maximum rather than the e-folding radius. (They are related by $r_{1/2} = \sqrt{-\log(1/2)}r_e$.)

The z-direction turbulent velocity is plotted in Fig. 7. The model results can be seen to lie at the lower end of the laboratory data, appropriately because this data corresponds to $z = 15$ and $z = 20$, while the higher data corresponds to $z > 50$, outside our model domain. the implication here is that we have not truly reached the self-similar region despite the match for the mean statistics. It is unlikely that subgrid scale would contribute significantly to these values.

Turbulent momentum transport (Fig. 8) is an even closer match - well within the spread of both model and data. The subgrid contribution has been computed here and can be seen to have little bearing on the total turbulent transport. An observation worth making is that the maximum subgrid transport appears to be near $r/r_{1/2} = 1.2$ which corresponds to $r/r_e = 1$, the point of maximum mean $\frac{\partial U}{\partial r}$.

The turbulent tracer transport (Fig. 9) is perhaps the least satisfactory comparison. the model results do sit in the region of one of two data sets - notably not the higher one which includes some co-flow. However the spread appears a little wide and the peak appears too close to the axis.

Two other comparisons were made but are not shown here. They were u_{rms}/u_{rms}_m and T_{rms}/T_{rms}_m, where the subscript m signifies a centerline value. In both cases the match to data was excellent (better than that shown Figs. 7 and 9) and it leaves open the question as to why Fig. 9 did not show a better match.

3.4. *Plume modeling*

The model was then run with the same boundary conditions and with buoyancy switched on ($Gr \neq 0$). The mean z-direction velocity and temperature show the same sort of excellent collapse by fitting Gaussian profiles and the centerline decay matches the slopes of $z^{-1/3}$ for U_m and $z^{-4/3}$ for T_m as expected from laboratory data of many sources. However the growth of the plume width is about 25% lower than expected and recent effort has been targeting the reason for this mismatch. Three candidates have come to mind - (i) failure of the Boussinesq assumption, (ii) misapplication of the stress-free lateral boundary condition, and (iii) an error in the model for the (now active) tracer.

3.4.1. *The Boussinesq assumption*

Of the several requirements for this assumption to hold (see Tritton, 1988) one is that the relative density difference $\delta\rho/\rho$ should be much lower than unity. However our numerical model was set up to match a particular data set of Shabbir & George (1994) who induced buoyancy by heating air to about 300^oC. Near the source $\delta\rho/\rho$ is about one, well outside the range for which Boussinesq should apply.

To check whether this could cause the narrowing of the numerical plume we lowered Gr from 9.25×10^6 to 2×10^5, a value well within the Boussinesq range and furthermore, one which should result in an initially momentum-dominated jet transitioning to a buoyancy plume within the model domain.

However the jet width remains too narrow, particularly towards higher z where buoyancy would be taking over from momentum as the dominant driving mechanism. While the density differences in the original model are high near the source, the Boussinesq assumption would be applicable over most of the domain and hence this would not significantly affect the results.

3.4.2. *The stress-free lateral boundary condition*

Given that our problem is apparently related to entrainment it is natural to examine the lateral boundary condition and the uniform pressure assumption. From the laboratory data and integrals models we know that whereas entrainment for a jet is constant, for a plume it increases with z. We explore this issue by developing simple irrotational flow models for the entrainment fields. The assumptions are: velocity and pressure are zero at $r = \infty$, there is a reflection at $z = 0$, along the axis ($r = 0$) there is a line sink with strength matching that found from integral models. The zone of flow establishment is ignored. The solutions are found by superposition of point sinks (Batchelor, 1970).

For the jet, the sink strength is given by $m = -0.25 W_0 \sqrt{A}$ where A is the area of the inlet (Fischer *et al.*, 1979), and the entrainment velocities are $U = 0$ for the z-component and $V = m/(2\pi r)$ for the r-component.

For the plume, the sink strength is $m = -0.155/3 B^{1/3} z^{2/3} = -a z^{2/3}$ (Fischer *et al.*, 1979), where $B = \delta\rho/\rho g U_0 A$ is the initial buoyancy flux. The entrainment velocities are found by numerically integrating the following expressions (the singularities in these integrals at $z = 0$ and $z = \infty$ are managed by appropriate transformations.):

$$U = \frac{a}{4\pi} \int_{-\infty}^{\infty} \frac{(z - z\prime) z\prime^{2/3}}{(r^2 + (z - z\prime)^2)^{3/2}} dz\prime$$

$$V = \frac{a}{4\pi} r \int_{-\infty}^{\infty} \frac{z\prime^{2/3}}{(r^2 + (z - z\prime)^2)^{3/2}} dz\prime$$

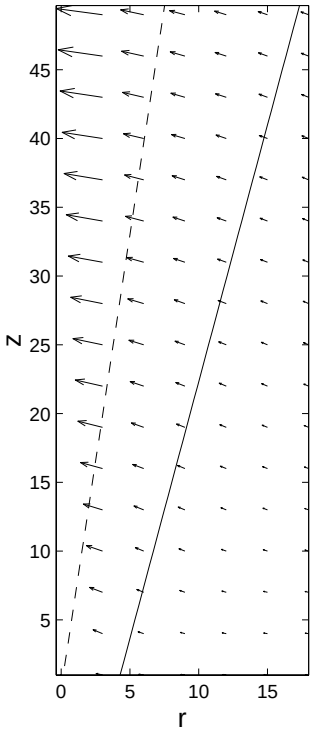

FIGURE 10. Entrainment flowfield predicted by a linesink model for a pure plume. The dashed line is the approximated edge of a plume (2σ). The solid line is the model boundary.

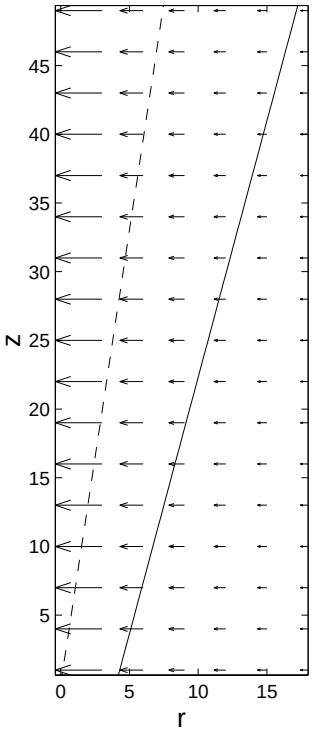

FIGURE 11. Entrainment flowfield predicted by a linesink model for a pure jet. The linestyles match Fig. 10

The solutions have been checked for consistency with the entrainment velocities for integral jet and plume models (i.e. the radial velocities at the e-folding radius match) and hence we can be confident of the applicability of these line sink solutions for the whole of the entrainment region including at the model boundary.

An examination of the velocities at the lateral boundary shows (Fig. 10) that there is a tangential component. With little curvature in the streamlines that means that there is indeed a pressure gradient along the boundary and hence the stress-free assumption is not strictly correct. However this true for the jet model as well (Fig. 11) and if the inaccuracy of the boundary condition were to cause the too-narrow plume then it should do so for both models. Therefore it appears that this is not a factor in the plume width problem and it may be that the generous volume of the entrainment region in the model allows circulation to adjust for the slight error at the boundary.

In fact the jet model does produce θ-direction boundary velocities consistent with those predicted by the line sink model (Fig. 12).

4. Future plans

Elimination of the Boussinesq approximation and the stress-free boundary conditions as culprits in the erroneous plume result leaves us with the third candidate - the subgrid

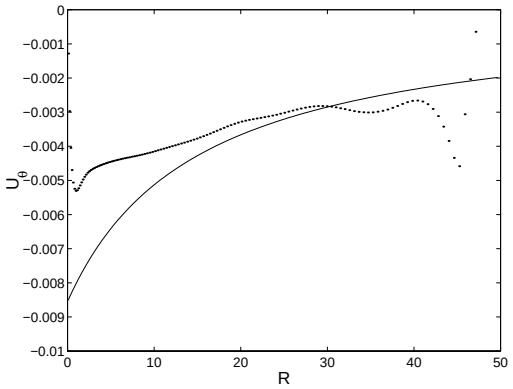

FIGURE 12. Normal velocity at lateral boundary. The points are the average model velocities, while the solid line has been obtained from a line-sink model.

scalar model. We have assumed that the subgrid diffusivity can be scaled from the subgrid viscosity using a constant Prandtl number of 0.7. Other experiments with LES models have found that lower Prandtl numbers, about 0.4, are consistently obtained for a range of molecular Prandtl numbers (Moin *et al.*, 1991). We will experiment with a range of Prandtl numbers. We can go further, however, and build in an explicit model for the subgrid diffusivity. In a way this would be more satisfying in that it would remove the imposition of what could be viewed as a tuning parameter which may be dependent on such things as the dimension of the LES filter.

Acknowledgment

Tony Webb's sabbatical stay at Stanford/NASA AMES is supported in part by CTR.

REFERENCES

BASTIAANS, R. J. M., RINDT, C. C. M., VAN STEENHOVEN, A. A. & NIEUWSTADT, F. T. M. 1994 Direct and large-eddy simulations of transient buoyant plumes: a comparison with an experiment, in P.R. Voke *et al.*(eds), *Direct and Large-Eddy Simulation I*, Kluwer Academic Publishers. 399-410

BASU, A. J. & MANSOUR, N. N. 1999 Large eddy simulation of a forced round turbulent buoyant plume in neutral surroundings. *Annual Research Briefs*, Center for Turbulence Research, NASA Ames/Stanford Univ. 239-248.

BATCHELOR, G. K. 1970 *An Introduction to Fluid Mechanics.* Cambridge U Press.

BOERSMA, B. J., BRETHOUWER, G. & NIEUWSTADT, F. T. M. 1998 A numerical investigation on the effect of the inflow conditions on the self-similar region of a round jet. *Phys. Fluids.* **10**, 899-909.

CABOT, W. & MOIN, P. 1996 Large eddy simulation of scalar transport with the dynamic subgrid-scale model. In *Simulation and modelling of turbulent flows*, (ed. Gatski T. B., M. Y. Hussaini, J. L. Lumley), Oxford University Press.

CHEN, C. J. & RODI, W. 1980 *Vertical turbulent buoyant jets, a review of experimental data.* HMT, the science and applications of heat and mass transfer, vol. 4, Pergamon Press.

Chorin, A. J. 1968 Numerical solution of the Navier-Stokes equation. *Math. Comput.* **22**, 745-.

Fatica, M., Orlandi, P. & Verzicco, R. 1994 Direct and large eddy simulations of round jets. In P. R. Voke *et al.*(eds), *Direct and Large-Eddy Simulation I*, Kluwer Academic Publishers. 49-60.

Fischer, H. B., List, E. J., Koh, R. C. Y., Imberger, J. & Brooks, N. H. 1979 *Mixing in inland and coastal waters.* Academic Press.

Germano, M., Piomelli, U., Moin, P. & Cabot, W. H. 1991 A dynamic subgrid-scale eddy viscosity model. *Phys. Fluids.* **A3**, 1760-1765.

Gresho, P. M. 1991 Incompressible fluid dynamics: some fundamental formulation issues. *Ann. Rev. Fluid Mech.* **23**, 413-454.

Kim, J. & Moin, P. 1985 Application of a fractional-step method to incompressible Navier-Stokes equations. *J. Comp. Phys.* **59**, 308-323.

Lilly, D. K. 1992 A proposed modification of the Germano subgrid-scale closure method. *Phys. Fluids.* **A4**, 633-635.

List, E. J. 1982 Mechanics of turbulent buoyant jets and plumes. In W. Rodi (ed) Turbulent buoyant jets and plumes, HMT, the science and applications of heat and mass transfer, vol. 6, Pergamon Press. 1-68.

Liu S., C. Meneveau and J. Katz 1994 Experimental study of similarity subgrid-scale models of turbulence in the far-field of a jet. In P.R. Voke *et al.* (eds), *Direct and Large-Eddy Simulation I*, Kluwer Academic Publishers. 37-48.

Moin, P., Squires, K., Cabot, W. & Lee, S. 1991 A dynamic subgrid-scale model for compressible turbulence and scalar transport. *Phys. Fluids A.* **3**, 2746.

Papantoniou, D. & List, E. J. 1989 Large scale structure in the far field buoyant jets. *J. Fluid Mech.* **209**, 151-190.

Piomelli, U. & Chasnov, J. R. 1996 Large-eddy simulations: theory and applications. M. Hallbäck *et al.* (eds), *Turbulence and transition modelling*, Kluwer Academic Publishers. 269-336.

Ricou, F. P. & Spalding, D. B. 1961 Measurements of entrainment by axisymmetric turbulent jets. *J. Fluid Mech.* **11**, 21-32, (1961)

Rodi, W.(ed) 1982 *Turbulent buoyant jets and plumes.* HMT, the science and applications of heat and mass transfer, **6**, Pergamon Press.

Shabbir, A. & George, W. 1994 Experiments on a turbulent buoyant plume. *J. Fluid Mech.* **275**, 1-32.

Tritton, D. J. 1988 *Phys. Fluid Dyn.* Clarendon Press.